A Multifuntional Nanoplatform Based on Responsive Fluorescent Plasmonic ZnO-Au@PEG Hybrid Nanogels

*Weitai Wu, Jing Shen, Probal Banerjee, and Shuiqin Zhou**

Under a rational design, combining multiple constituents into a single nano-object will not only bridge the unique properties of individual materials to leverage research both fundamentally and practically, but will also improve conventional sensing, imaging, and therapeutic efficacies. Such a nano-object (<100 nm) can be constructed by covalently bonding ZnO quantum dots (QDs) to nonlinear poly(ethylene glycol)-based nanogel network chains, followed by appropriate growth of metallic Au. With the polymer gel network serving as a three-dimensional scaffold, the fluorescence of ZnO QDs can be well protected, while metal Au still retains its surface plasmon resonance property. The ZnO QDs covalently bonded to the thermo-responsive gel network chains can sensitively respond to temperature change of the surrounding fluids over the physiologically important range of 37–42 °C, converting the disruptions in homeostasis of local temperature into stable, robust and high-resolution fluorescent signals. The thermoresponsive hybrid nanogels can not only enter into and light up B16F10 cells, but also regulate the release of a model anticancer drug, temozolomide, in response to either local environmental temperature change or external near-infrared light-induced localized hyperthermia from metal Au. The combined chemo-photothermal therapy can significantly improve the therapeutic efficacy due to a synergistic effect.

1. Introduction

The ability of a single object to perform multiple functions is often cited as an advantageous characteristic of nanoplatforms that cannot be achieved with the individual constituents. Specific integration of different building blocks with desired optical, electronic, and collective properties into a single structure has resulted in novel platforms of materials that may lead the way to various future technologies, such as chemical and biochemical sensing,[1] multimodal imaging,[2] and simultaneous diagnosis and therapy.[3] Fluorescence is by far the most powerful method for in vitro and in vivo detection, because it can be noninvasive and workable in even strong electromagnetic fields. Among various kinds of materials, semiconductor quantum dots (QDs) as fluorescent probes have attracted increasing interest due to their high quantum yield, photostability, and wideband excitation.[4] Recently, fluorescent hybrid nanogels, which are capable of transducing volume phase transitions into a change in fluorescence intensity, have been constructed by the physical incorporation of QDs into stimuli-responsive polymer networks by our group[5] and others.[6] On the other hand, Au nanoparticles (NPs) constitute another major class of nanomaterials. Metallic Au has promising therapeutic properties as a hyperthermal agent due to its efficient photo-to-heat conversion ability, which can induce a local temperature increase around Au NPs under light illumination through the tunable surface plasmon resonance (SPR) bands in the near-infrared (NIR) region.[7] Au NPs have also been used for NIR-controlled release of anticancer drugs. Covered with temperature-responsive polymers, the Au NPs can convert the NIR light to heat that can induce the responsive polymers to collapse, which further trigger the release of the pre-loaded drugs.[3b,8,9] Fluorescent temperature sensing is necessary in hyperthermal and photodynamic cancer therapies because knowing the temperature of Au-based drug carriers and pathological tissue is essential in order to achieve optimal therapeutic results. Moreover, pathological cells are warmer than normal cells by 1–5 °C because of their enhanced metabolic activity,[10] which was demonstrated for the first time in Uchiyama's group using an organic fluorophore-contained nanogel as an intracellular thermometer.[11] Integration of thermometry with the thermally/photothermally controllable drug release into a single nano-platform can contribute to the explanation of intricate biological processes and the development of novel diagnoses and therapies.[12] Although considerable research efforts have been put into various fields, unfortunately, no report of any drug carriers drawing the merits of both QDs (high quantum yielded fluorescence) and Au (plasmonics) for common progress has appeared in the literature.

Retaining the unique properties of each building block after nanoscale integration is a long-standing problem.[13] It is

Dr. W. T. Wu, J. Shen, Prof. S. Q. Zhou
Department of Chemistry
College of Staten Island of The City University of New York
Staten Island, New York 10314, USA
E-mail: shuiqin.zhou@csi.cuny.edu
Prof. P. Banerjee
Department of Chemistry and CSI/IBR Center
for Developmental Neuroscience
College of Staten Island of The City University of New York
Staten Island, New York 10314, USA

DOI: 10.1002/adfm.201100201

© 2011 WILEY-VCH Verlag GmbH & Co. KGaA, Weinheim

particularly difficult to combine the fluorescence of QDs with the plasmonic property of metals such as Au.[14] The combination of QD fluorescence with Au plasmonics has been demonstrated on flat surfaces.[15] However, the direct growth of Au onto single QDs, quantum rods or tetrapods usually leads to a quenching in either the photonics or plasmonics of the constructed QD-Au NPs.[13,16] Very recently, inspired by the biomineralization of Au,[17] Jin and Gao successfully combined the fluorescence and plasmonics into a single Au-shell-encapsulated CdSe/ZnS QD by using poly(ethylene glycol) (PEG)-based linear polymer chains as a structural scaffold.[2a] The spacing between the QD core and Au shell was controlled by engineering the polymer intermedius through layer-by-layer assembly. As a consequence, a high photoluminescence quantum yield (PLQY) of ≥39% of the QDs and a strong surface plasmon scattering of the Au shell were simultaneously achieved, making the nanoplatform an excellent dual-modality imaging agent.

In this work, we design a thermoresponsive nonlinear PEG-based polymer nanogel network to act as a three-dimensional (3D) scaffold to integrate ZnO QDs and metallic Au into a single hybrid nanogel particle (<100 nm). As schematically depicted in **Figure 1**a – coupled with a specific physiochemical characteristic, the disruption in homeostasis of local temperature – the newly designed nanoplatform combining the building blocks of fluorescent QDs, plasmonic metal Au, and responsive polymer gels should provide great potential for biomedical applications. We demonstrate that the tri-component hybrid nanogels, denoted as ZnO-Au@PEG, display cooperative properties while maintaining the individual properties of each constituent, thus allowing the integration of three important applications: ratiometric fluorescent sensing of temperature change in physiological fluid, fluorescent cell imaging, and thermal/photothermal-regulated drug delivery. Unlike our previously studied biosensors with CdSe QDs physically restricted in polysaccharide-based gel networks,[5] the newly developed hybrid nanogels with ZnO QDs covalently bonded to the PEG-based gel network chains can prevent the liberation of QDs when applied for analysis of biological fluids under varying environments, thus providing high sensitivity and long-term reproducibility. A stable and highly accurate photoluminescence (PL) response is important for future in situ studies in bio-systems. Furthermore, concerning the long-term toxicity that may be caused by the release of Cd ions from cadmium-based QDs, ZnO QDs are believed to be more versatile for bio-applications.[4b,4c] Inspired by Uchiyama's intracellular thermometer,[11] we anticipate that the novel ZnO-Au@PEG hybrid nanogels could be potentially used as intelligent fluorescent labels to monitor local temperature changes in tumors, standing in contrast against conventional labels, which are insensitive to local environmental change. In addition, hybrid nanogels could also be developed for simultaneous chemo and photothermal cancer treatment, where either the local pathological temperature change (endogenous activation) or NIR-induced localized hyperthermia (exogenous activation) can provide spatiotemporal control of the release of the anticancer drug temozolomide (TMZ) from the hybrid nanogel carriers. The interdisciplinary design and development of multifunctional intelligent nano-platforms would pave a new path in biological manipulation, medical diagnosis and therapy.

2. Results and Discussion

2.1. Synthesis and Structure of ZnO-Au@PEG Hybrid Nanogels

The strategy to prepare the multifunctional ZnO-Au@PEG hybrid nanogels involves first the synthesis of ZnO@PEG hybrid nanogels, followed by a moderate growth of Au nanoclusters inside the hybrid nanogels. The ZnO@PEG hybrid nanogels were synthesized from the copolymerization of zinc methacrylate ($Zn(MAA)_2$), 2-(2-methoxyethoxy)ethyl methacrylate (MEO_2MA), oligo(ethylene glycol)methyl ether methacrylate (MEO_5MA), and a crosslinker poly(ethylene glycol) dimethacrylate (PEGDMA) in ethanol and then transferred into aqueous solution. In the FTIR spectrum (**Figure 2**a), the characteristic absorption for the bridging coordination modes of acetate group with Zn appears at 1600 cm^{-1} (C=O) and 1443 cm^{-1} (C–O),[4b,4c,18] respectively, indicating that ZnO QDs were covalently connected to the gel network chains. The signal at about 1726 cm^{-1} is assigned to the –COOR and –COOH groups, and the broad band at 1050–1150 cm^{-1} (C–O–C) is associated with the PEG chains. The covalently immobilized ZnO QDs can emit a relatively weak near-UV light (393 nm, assigned to exciton recombination) and a strong yellow-green light (530 nm, vacancy PL) in aqueous solution (Figure 2b). To introduce Au into the nanogels, $HAuCl_4$ was used as the precursor. Wang et al.[16b] found that citrate-capped ZnO nanocrystals could act as centers for the reduction of Au(III) by citrate and then form nucleation sites for reduced Au atoms; however, no reaction was observed in the citrate/$HAuCl_4$ solution in the absence of ZnO nanocrystals. In our case, the ZnO QDs covalently immobilized in the nanogel networks were applied as nucleation sites for the growth of metallic Au to synthesize ZnO-Au@PEG hybrid nanogels under dark and in an ice bath. The control experiment indicated that the reduction of Au(III) to Au(0) is very slow in water or in the dispersion of the nonlinear PEG-based nanogels that contain no ZnO QDs (at least no evidence was observed in UV–vis–NIR spectra after a week), which minimizes the rapid nucleation of monometallic Au that are located inside the gel networks but

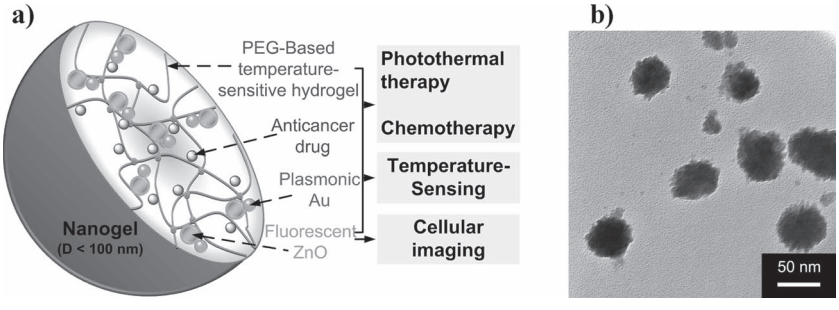

Figure 1. a) Model of the tri-component responsive hybrid nanogels for multifunctional applications in biomedicine. b) Typical TEM image of ZnO-Au@PEG hybrid nanogels (ZAG-2).

© 2011 WILEY-VCH Verlag GmbH & Co. KGaA, Weinheim

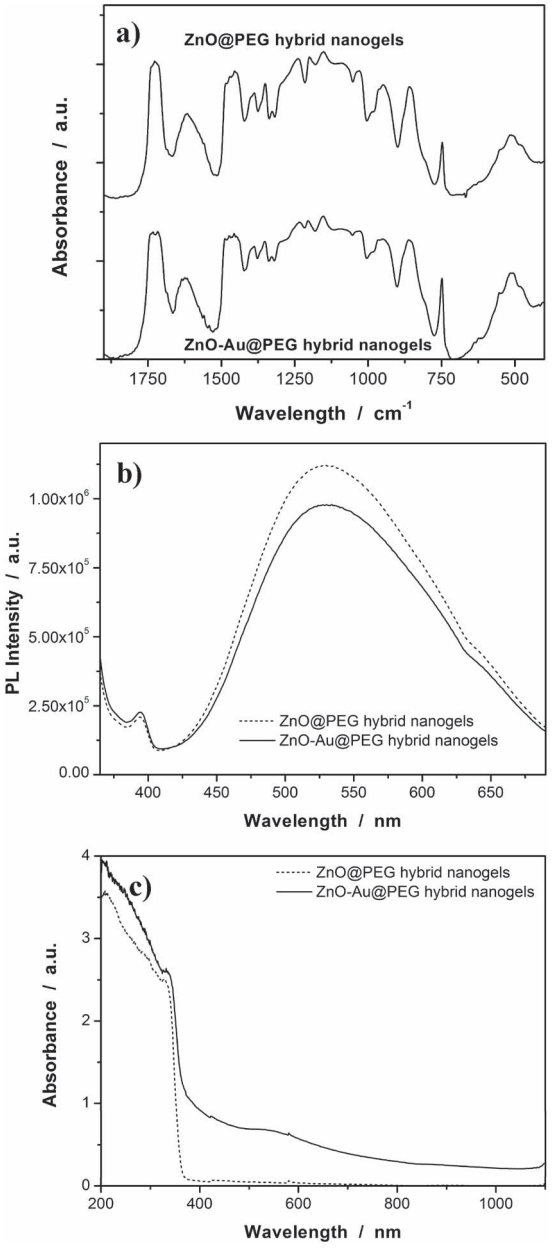

Figure 2. a) Typical FTIR spectra, b) PL profiles, and c) UV–vis–NIR absorption spectra of ZnO@PEG and ZnO-Au@PEG hybrid nanogels (ZAG-2) recorded at room temperature.

unassociated with ZnO QDs. Interestingly, as shown in Figure 2c, the metallic Au incorporated in our hybrid nanogels exhibited a typical SPR band at aroudn 525 nm and trailed to NIR region, standing in vivid contrast against the faintly seen SPR in the directly coupled ZnO-Au NPs.[16b] FTIR spectroscopy indicated a slight split in the IR signals of C=O in the –COOZn and –COOH groups for our ZnO-Au@PEG hybrid nanogels. However, no evident change was observed for the C–O or C–O–C signals. These results suggested a higher accessibility of Au(III) ions and subsequently the growth of metallic Au on the C=O regions than on the C–O or C–O–C regions. Nevertheless, the obtained ZnO-Au@PEG hybrid nanogels show great stability. No sediment was observed even after 6 months storage at room temperature (approximately 22 °C). Only a marginal change in UV–vis–NIR absorption can be detected for both ZnO and Au (see Figure S1 in the Supporting Information), implying that the size of ZnO and Au remained unchanged during storage. The stable SPR of ZnO-Au@PEG hybrid nanogels are desirable for their successful use in NIR-controlled drug release.

A key question was then whether the ZnO QDs in ZnO-Au@PEG hybrid nanogels would remain fluorescent. As shown in Figure 2b, a slight enhancement in 393 nm emission accompanied by a quenching in 530 nm emission was observed for ZnO-Au@PEG hybrid nanogels, in comparison with ZnO@PEG hybrid nanogels. The emission peak positions did not shift. It is known that the optical property of a material is closely associated with its electronic structure. At short separation distance and significant overlap between QD emission and Au SPR bands, Au NPs have been demonstrated as fluorescence quenchers of QDs.[2a,13,16] The Fermi energy level of Au is higher than that of ZnO due to the smaller work function of Au (5.1 eV) than ZnO (5.2–5.3 eV),[16a] so that the electron transfer from Au to the closely contacted ZnO would occur until the two systems attain equilibration. Considering that surface plasmon energy of metal Au matches well with the emitted visible photon energy of ZnO QDs, the emitted photons can produce the surface plasmon through energy transfer, which promotes electrons in Au to an excited state by a surface plasmon wave. The excited electrons will subsequently tunnel into the conduction band of ZnO parts. A similar but more significant spectral change has been observed on the ZnO-Au composites, in which the near-UV emission was enhanced by one order of magnitude compared to that of pure ZnO NPs, accompanied by a weakened visible emission to about two-thirds that of pure ZnO NPs.[16b] In contrast, with the polymer gel network serving as a 3D scaffold, the ZnO QDs in the ZnO-Au@PEG hybrid nanogels showed only a slightly decreased PLQY at 530 nm and a similar PLQY at 390 nm as compared to the ZnO QDs in the template ZnO@PEG hybrid nanogels. In comparison with other Cd-free QDs,[4d,4e] the ZnO QDs in the ZnO-Au@PEG hybrid nanogels still possess a considerably high PLQY (approximately 23%) at 530 nm.

The transmission electron microscopy (TEM) images show that ZnO-Au@PEG hybrid nanogels are nearly spherical and smaller than 100 nm in size (Figure 1b for ZAG-2, see Figure S2 in the Supporting Information for others). The overall size of the four hybrid nanogels ZAG-1 (45 nm), ZAG-2 (58 nm), ZAG-3 (76 nm), and ZAG-4 (98 nm) correspondingly increased when the feeding of the MEO_5MA monomers was gradually increased while the amount of MEO_2MA was fixed during synthesis. On the basis of physiological parameters, such as hepatic filtration, tissue extravasation, tissue diffusion, and kidney excretion, it is clear that carrier particle size is a key factor to achieve long circulation for good biodistribution and high therapeutic efficacy.[19] NP-based drug carriers in the size range of 10–100 nm have actual advantages to improve the blood circulation time and enhance the extravasation rate into permeable tissues such as tumors.[19,20] Since the polymer chains occupy more than 80% of the dried particle volume and

© 2011 WILEY-VCH Verlag GmbH & Co. KGaA, Weinheim

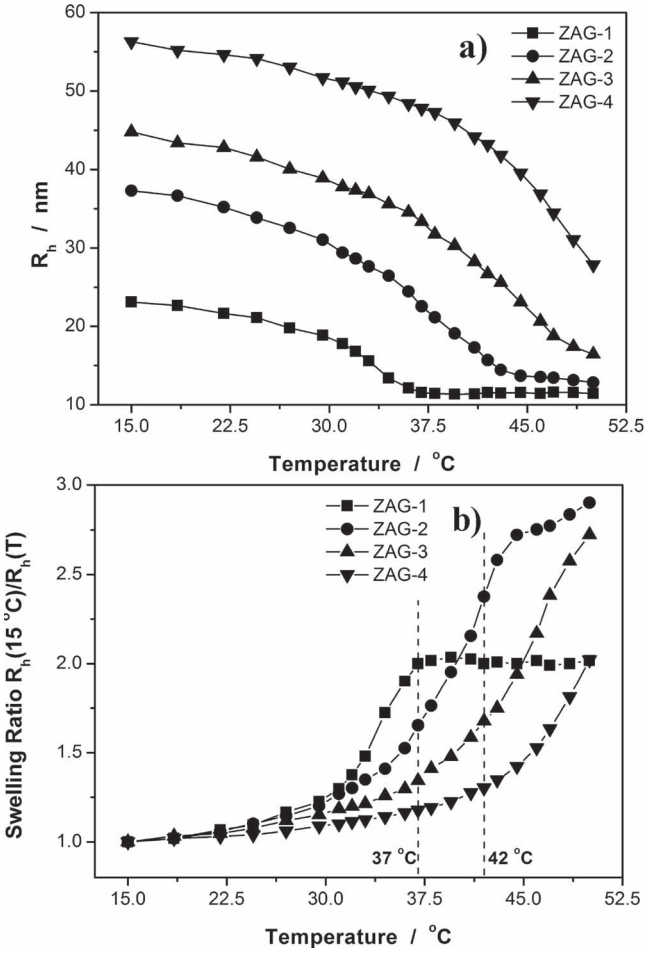

Figure 3. a) Temperature dependence of the average R_h values, and, b) swelling ratio, $R_h(T)/R_h(15.5\ °C)$, of ZnO-Au@PEG hybrid nanogels ZAG-1 (■), ZAG-2 (●), ZAG-3 (▲), and ZAG-4 (▼) in PBS of pH = 7.4, measured at a scattering angle $\theta = 90°$.

TEM image is a 2D projection for a 3D distribution of the ZnO QDs/Au inside the nanogels, the structure of the immobilized QDs/Au cannot be seen clearly. As the size of QDs is directly related to the excitonic peak in the UV–vis–NIR absorption spectrum, the size of ZnO QDs can be estimated by empirical functions reported by Meulenkamp.[21] The typical $\lambda_{½}$ of ZnO QDs (Figure 2c), the wavelength at which the absorption is 50% of that at the excitonic peak (or shoulder), is determined as about 348 nm for all the studied samples before and after the growth of Au, from which the average size of ZnO QDs was calculated to be about 3.5 nm.

2.2. Temperature-Induced Volume Phase Transition

The ZnO-Au@PEG hybrid nanogels can undergo a reversible temperature-responsive volume phase transition (**Figure 3**). The swelling/deswelling characteristic is a consequence of the counterbalance of the hydrophilic and hydrophobic forces in the nanogels at particular temperatures. The polymers made from MEO_2MA and MEO_5MA have lower critical solution temperatures (LCST) of about 24 and 61 °C, respectively. The equilibrium swelling ratio of the copolymerized gel networks can be regulated by the feeding molar ratio $r_{mol} = n_{MEO2MA}/n_{MEO5MA}$ in the synthesis, leading to a shift in the critical volume phase transition temperature (VPTT) of the hybrid nanogels.[9b,22] The higher the r_{mol}, the lower the VPTT of the hybrid nanogels. While ZAG-1 (r_{mol} = 2.21) and ZAG-4 (r_{mol} = 0.65) exhibited a VPTT at approximately 34 and >50 °C, respectively, a proper control of r_{mol} in ZAG-2 (r_{mol} = 1.31) and ZAG-3 (r_{mol} = 0.89) resulted in a continuous change in hydrodynamic radius (R_h) but of tunable slopes across the physiologically important temperature range of 37–42 °C that are found in many pathological zones, such as in tumors.[10,11]

2.3. Temperature-Sensitive PL Property of ZnO-Au@PEG Hybrid Nanogels

Having demonstrated that ZnO-Au@PEG hybrid nanogels could retain the QD fluorescence, Au plasmonics, and PEG thermosensitivity after nanoscale integration, we next examine the cooperation of these properties for multifunctional applications. The responsive ZnO-Au@PEG hybrid nanogels can convert the temperature changes into optical signals in terms of the visible emission intensity change of ZnO QDs (**Figure 4**). Simply placed in a container and irradiated with a 375 nm UV lamp, the hybrid nanogel dispersions exhibit different color at 15.5 and 50.0 °C, observable by the naked eye (photographs in Figure S3 in the Supporting Information). More robust signals can be obtained by using the enhanced PL intensity $I(T)/I(15.5\ °C)$, where $I(T)$ is the PL intensity at 530 nm recorded at different temperature T. In comparison with the R_h–temperature plot (Figure 3b), the $I(T)/I(15.5\ °C)$ reveals nearly the same trend towards temperature change (Figure 4b), clearly correlating the temperature-induced volume change of the nanogel to the PL response of QDs. Two factors should be considered to explain how the temperature-induced shrinking of nanogels could trigger the PL enhancement of the immobilized QDs. One is related to an increase in the local refractive index around the QDs during the collapse of the nanogel, which could affect the quantum efficiency of QDs.[23] Another is related to the variation of the strain at the surface of QDs. At low temperatures, the cross-linked structure hinders the volume expansion at a high swelling state, creating elastic tensions localized at the cross-linking points. Because the ZnO QDs are covalently bonded to the polymer chains, the QDs also act as cross-linking points. Thus, the elastic tension will propagate to the surface of the QDs, producing surface quenching states.[24] The increase in temperature induces the gel to shrink, which can diminish the elastic tension and consequently reduce the number of quenching centers, leading to an enhancement in PL intensity. The optical response is completely reversible (Figure 4c). Since the PL response is triggered by the volume phase transition of the nanogels, the kinetics of the PL response will depend on how fast the volume phase transition is. The rate of stimuli-induced volume phase transition of a hydrogel particle is scaled as l^{-2}, where l is the relevant length of gel particle.[25] Nanosecond to microsecond (approximately 100 ns) volume phase transitions have been determined for individual temperature-responsive

© 2011 WILEY-VCH Verlag GmbH & Co. KGaA, Weinheim

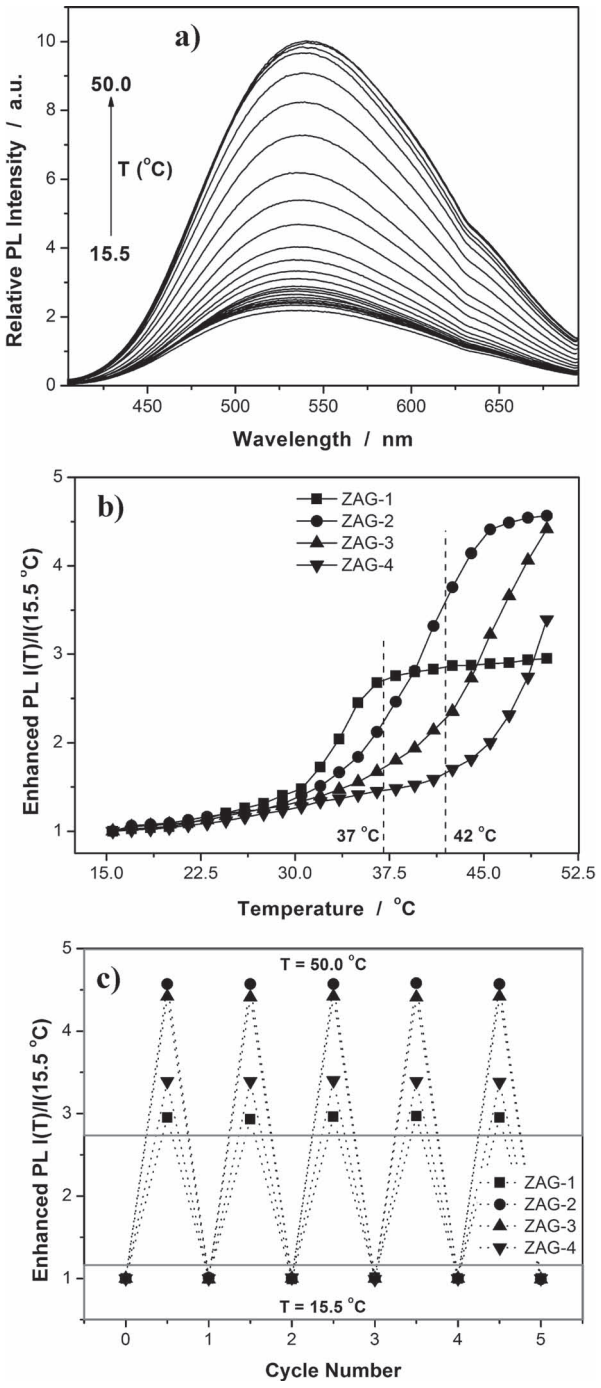

Figure 4. a) Typical PL spectra of ZnO-Au@PEG hybrid nanogels (ZAG-2) at different temperatures. Scans were taken at 1.5 °C intervals from bottom to top, from 15.5 to 50.0 °C. b) The temperature-induced PL intensity enhancement, $I(T)/I(15.5\ °C)$, measured at 530 nm. c) Enhanced PL of the hybrid nanogels during repeated heating (50.0 °C) and cooling (15.5 °C) cycles. All measurements were made in 0.005 M PBS of pH = 7.4. Excitation wavelength = 340 nm.

poly(*N*-isopropylacrylamide) nanogel particles in the size range of around 200–350 nm.[26] The kinetics of the temperature-induced phase transition of the sub-100 nm ZnO-Au@PEG hybrid nanogels should be in the 100 ns scale or even faster. Thus, our hybrid nanogels should be able to undergo a very fast PL response to a temperature change. Furthermore, with a precision of ±1% in the determination of the PL intensity, a temperature resolution of ±0.18–0.24 °C can be achieved for ZAG-2 over the range 37–42 °C, which is very close to the one achieved on the conformational response of a temperature-responsive polymer chain.[27] The temperature resolution or the sensitivity of PL response can be fine-tuned through the control of the temperature-responsive volume phase transition of the PEG-based networks (Figure 4b). In comparison with previously studied hybrid nanogels with the QDs/NPs physically restricted in the interior of the polymer networks,[5,9b] the present ZnO-Au@PEG hybrid nanogels demonstrate a much higher sensitivity of PL response, possibly due to the rapid and sensitive transmission of the elastic tension directly from the polymer chains to the covalently bonded QDs. The rapid and highly accurate PL response will be an important feature for future in situ studies in biosystems.

To examine the potential interference from ion strengths, NaCl was used as an ion source to mimic intracellular conditions, as Na^+ (approximately 0.010 M) is the only component of the cellular growth medium required for the development and disappearance of vacuoles.[28] When the NaCl concentration increased from 0 to 0.200 M (Figure S3), an almost identical PL response to the temperature variation was obtained with a relative error less than ±0.52% over the range 37–42 °C, demonstrating a minimal impact of the ion strength on the signaling ability of the hybrid nanogels. The interference can be further eliminated when the enhanced PL intensity is expressed as the ratio of $I(T)/I(15.5\ °C)$ to evaluate the PL response. Similarly, the PL response was nearly independent of the environmental pH over 5.0–7.4 (±0.19%, Figure S4). This feature is desirable because the extracellular pH of a tumor environment and endosomal/lysosomal pH lie at approximately 7–6.5 and 6.5–5.0, respectively.[10] Therefore, high sensitivity and high selectivity for temperature sensing over a physiological range could be achieved on our Zn ZnO-Au@PEG hybrid nanogels.

2.4. Drug Loading and in vitro Thermal- and Photothermal-Regulated Drug Release

Three hybrid nanogels of ZAG-2, ZAG-3, and ZAG-4 with high temperature sensitivity over the physiological temperature range were selected for further in vitro experiments. TMZ, a new imidazole tetrazinone compound (Figure S5) with promising preclinical and clinical activity in nitrosourea-sensitive and nitrosourea-resistant models and manageable toxicity in phase I/II clinical trials,[29] was selected as a model drug for uploading into the hybrid nanogels (purified at 22 °C). With the high porosity of the gel and the hydrogen bonding interaction between the ether oxygens of PEG chains and the amide groups of TMZ, high drug loading capacities of 43.6, 48.9 and 55.3 wt-% were achieved for ZAG-2, ZAG-3 and ZAG-4, respectively. Fluorescent microscopy indicates that the drug-loaded hybrid nanogels still show strong fluorescence. TMZ has a negligible effect (+1.7%) on the PL enhancement ($I(T)/I(15.5\ °C)$) of the hybrid nanogels over the range 15.5–50.0 °C.

© 2011 WILEY-VCH Verlag GmbH & Co. KGaA, Weinheim

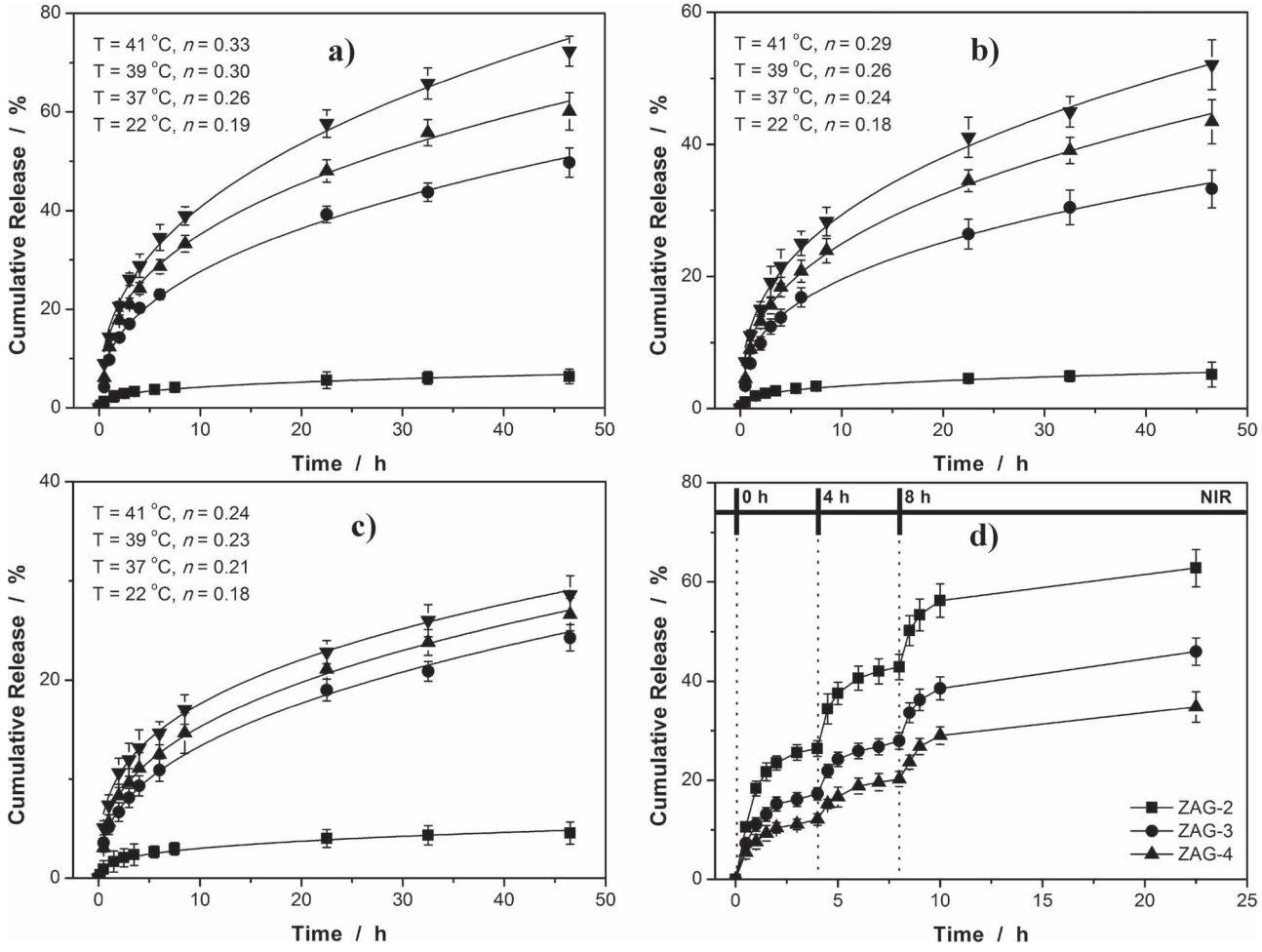

Figure 5. Release profiles of TMZ from ZnO-Au@PEG hybrid nanogels: a) ZAG-2, b) ZAG-3, and c) ZAG-4 in PBS at pH = 7.4 at different temperatures (22 °C: ■; 37 °C:●; 39 °C:▲; 41 °C: ▼). The lines are based on the fitting of Peppas's Model: $M_t/M_\infty = kt^n$. d) Release profiles of TMZ from ZAG-2, ZAG-3, and ZAG-4 immersed in PBS of pH = 7.4 at a constant temperature of 37 °C, upon exposure to 5 min of 1.5 W cm^{-2} NIR light for 0, 4, and 8 h.

Two approaches can be used to regulate the release of the pre-loaded TMZ from the hybrid nanogels. First, the increase in temperature of the releasing medium can speed up the release (**Figure 5**a–c). The releasing rate can be further tailored by engineering the phase behavior of the hybrid nanogels. ZAG-2, ZAG-3, and ZAG-4 with a gradual increase in VPTT exhibit a gradually decreased releasing rate. The releasing profiles fit well to Peppas's model:[30]

$$M_t/M_\infty = kt^n$$

where M_t and M_∞ are the cumulative amount of drug released at time t and infinite time, respectively, k is a structural/geometric constant, and n is related to the intimate mechanism of release. The calculated n values are all below the critical value of 0.43,[30] which indicates that the release from the sphere-like hybrid nanogels obeys two correlated processes: one is related to the breakage of hydrogen bonds between the drug and the gel network chains; another is a diffusion-controlled step. The increase in temperature from 22 to 41 °C increased the n value, but did not change the drug release mechanism. Such a temperature-dependent release profile may be exploited for biologically controlled drug release utilizing the abnormal temperature increase in pathological zones.[10,11] Drug release by a stepwise treatment also can be achieved after further modification, for example, simply by purifying the drug-loaded carriers at the normal temperature of 37 °C (Figure S5).

Second, NIR light can provide a highly orthogonal external stimulus, allowing spatiotemporally controlled release. The metal Au can absorb and convert NIR light into heat on a picosecond time scale, as a result of electron–phonon and phonon–phonon processes.[7] The heat will dissipate into the surroundings, and the rise in local temperature causes the shrinking of the gel networks, thereby accelerating the release of pre-loaded TMZ (Figure 5d), in comparison to cases without NIR irradiation. When the lamp is turned off, heating will immediately cease. The decrease in temperature will bring the polymer chains back to its original extended conformation, thus the drug release returns to its regular rate. During these procedures, the NIR irradiation (5 min,

© 2011 WILEY-VCH Verlag GmbH & Co. KGaA, Weinheim

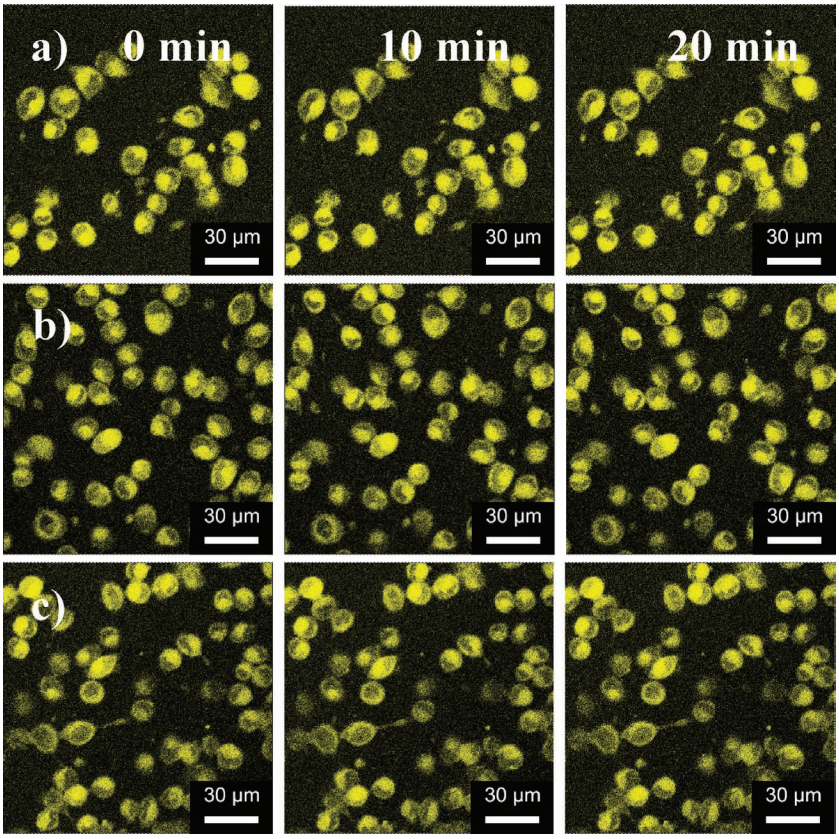

Figure 6. Scanning confocal images of B16F10 cells incubated with ZnO-Au@PEG hybrid nanogels: a) ZAG-2, b) ZAG-3, and c) ZAG-4. Excitation wavelength 405 nm.

1.5 W cm^{-2}) caused little temperature increase (far less than 1 °C) in the releasing medium. Such an NIR-triggered drug release should remarkably enhance the ability of our hybrid nanogels for specific drug delivery to the tumor site. Depending on the stage and type of cancer, this NIR-accelerated drug release can provide high dosage at a shorten treatment time if necessary.

2.5. Cell Internalization and Cell Viability of in vitro Chemo, Photothermal, and Chemo-photothermal Treatments

The ZnO–Au@PEG hybrid nanogels can emit strong visible fluorescence under the physiological conditions, which renders them useful for biomedical detection of the drug carriers and imaging diagnosis. Laser confocal microscopy was used to evaluate whether these hybrid nanogels could be used for tumor cell imaging. The hybrid nanogels show bright and colorful spots in the fluorescent imaging, while no significant autofluorescence was observed on the mouse melanoma cells B16F10. After incubation of the cells with the hybrid nanogels for 24 h, the difference in colors reflected the fact that the hybrid nanogels can penetrate into the living cells and exhibit bright fluorescence (**Figure 6**, also see Figure S6 and S7 in the Supporting Information), which can retain nearly the same PL intensity even after 20 min irradiation. These bright spots are mainly distributed in the cytoplasm and perinuclear region of the cells. As the complexity of molecular interactions governing endocytosis are revealed, the mechanisms of endocytosis should be viewed in a broader context than simple vesicular trafficking.[9b,20b,31] When the size of NPs is smaller than 100 nm, the biological pathways in cells can undergo profound changes.[31] Moreover, PEG chains are known to be able to serve as efficient steric protectors for various particulates (such as micelles, liposomes, and NPs) in biological media.[32] It has been reported that small-sized (<100 nm) PEG-phosphatidylethanolamine micelles can attain deep penetration into poorly permeable tumors.[20a] Nevertheless, it is obvious that these hybrid nanogel probes do not give dark regions in the cell, and simply areas where the nanogel did not permeate are clear, rendering them suitable for cell-labelling markers. Combining with the fluorescent signaling ability, one possible application of the hybrid nanogels is for intracellular sensing and imaging of temperature, which may be termed as intelligent labelling. It should be mentioned that our current experimental setup cannot record the intracellular temperature. Intracellular thermometry has been achieved on Uchiyama's instruments.[11]

A beautiful characteristic of ZnO-Au@PEG hybrid nanogels for future biological applications, especially for clinical applications, is the low cytotoxicity of each component. In Figure 6, no signs of morphological damage to the B16F10 cells were observed upon treatment with the hybrid nanogels, demonstrating minimal cytotoxicity. This was further supported by the fact that more than 95% of B16F10 cells can survive upon treatment with the hybrid nanogels with concentrations up to 114.6, 102.2 and 90.4 μg mL^{-1} for ZAG-2, ZAG-3 and ZAG-4, respectively (Figure S8). In contrast, the cell viability drastically decreased when the cells were treated with TMZ-loaded ZAG-2, ZAG-3 and ZAG-3 even at concentrations as low as 11.5, 10.2 and 9.0 μg mL^{-1}, respectively (equivalent to 25.8 μM free TMZ). These results indicate that the TMZ-loaded hybrid nanogels provide a high anticancer activity. The cytotoxicity of TMZ-loaded hybrid nanogels is lower than that of free TMZ solution at all the studied concentrations. This can be attributed to the sustained-release property of the TMZ-loaded hybrid nanogels. Considering that less than 40% of the loaded TMZ was released in 24 h under physiological conditions (Figure 5), the slightly lower cytotoxicity of the TMZ-loaded hybrid nanogels than the free TMZ solutions is understandable.

To investigate the effect of combined chemo-photothermal treatment, the cell viability was measured when the B16F10 cells were treated with drug-free and TMZ-loaded hybrid nanogels for 24 h, respectively, but adding 5 min initial NIR irradiation. The addition of initial 5 min NIR irradiation has a neglectable effect on the cytotoxicity of the free TMZ solutions or free ZnO-Au@PEG hybrid nanogels. Using the

© 2011 WILEY-VCH Verlag GmbH & Co. KGaA, Weinheim

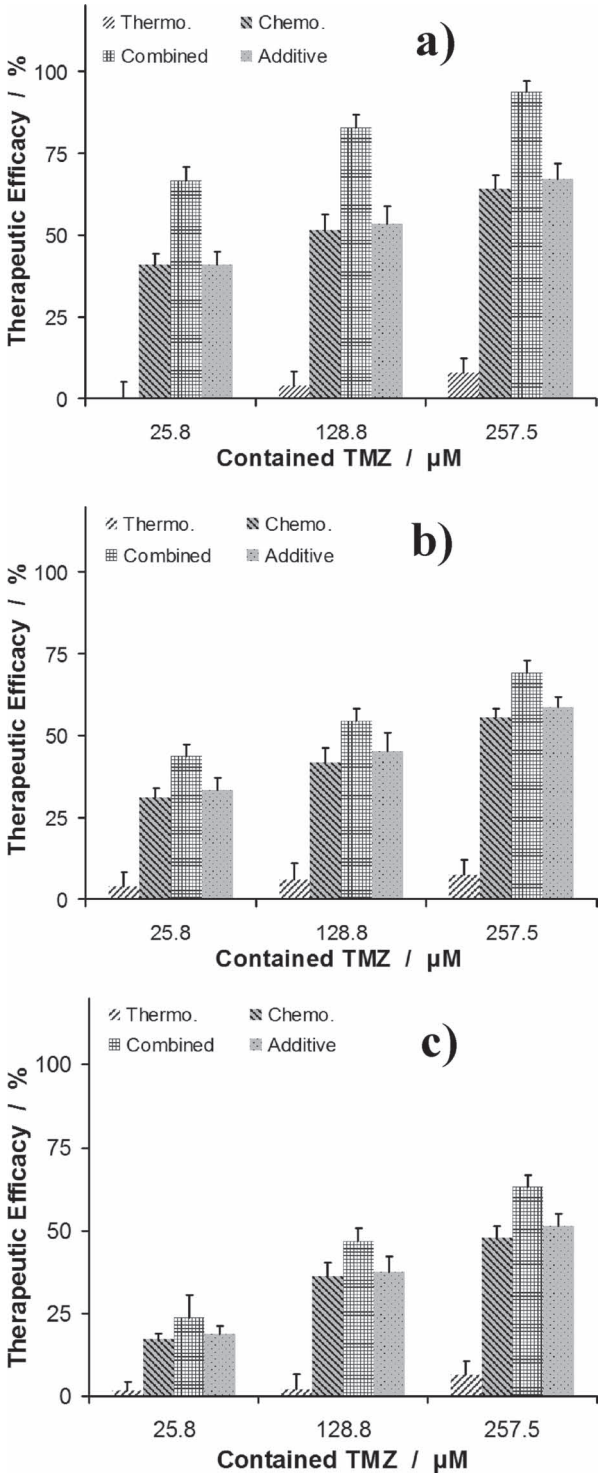

Figure 7. Therapeutic efficacies of photothermal, chemo, and combined chemo-photothermal treatments with ZnO-Au@PEG hybrid nanogels a) ZAG-2, b) ZAG-3, and c) ZAG-4 as drug carriers calculated by subtracting cell viability from 100%. Additive therapeutic efficacies of chemo and photothermal treatments were estimated using the relation of $T_{additive} = 100 - (f_{chemo} \times f_{photothermal}) \times 100$, where f is the fraction of surviving cells after each treatment. The efficacy of combined treatment is compared with the additive efficacy of independent chemo- and photothermal treatments using *t*-tests with all *p*-values lower than 0.05.

hybrid nanogels as drug carriers, the combined TMZ and photothermal treatment exhibited much higher therapeutic efficacy (calculated by subtracting the cell viability from 100%) than the chemotherapy or photothermal treatment alone (**Figure 7**). The efficacy of the combined TMZ-photothermal treatments is also significantly higher than the additive therapeutic efficacy of chemo- and photothermal treatments, which were estimated using the relation of $T_{additive} = 100 - (f_{chemo} \times f_{photothermal}) \times 100$ with f being the fraction of surviving cells after each treatment.[33] When a *t*-test is used to compare the efficacy of combined treatment with the efficacies of chemo- and photothermal treatments and their additive value, all *p*-values are lower than 0.05, indicating a significant difference. Clearly, the synergistic effect of chemo-photothermal treatment is demonstrated on ZnO-Au@PEG hybrid nanogels.

3. Conclusions

We have developed an advanced multifunctional nanoplatform that can be constructed by using polymer nanogel as a 3D scaffold to covalently bond ZnO QDs onto the thermoresponsive PEG-based gel network chains, and then appropriately growing metallic Au in the interior of the nanogels. Different to other examples of QD/NP-loaded nanogel colloids or QD/Au heterojunction structures in which metallic Au significantly quenched the fluorescence of QDs, the beauty of the newly developed ZnO-Au@PEG hybrid nanogels is that they can successfully integrate the strong fluorescence (PLQY ≈ 23%) of ZnO QDs, SPR of metal Au, and thermosensitivity of nanogel into a single sub-100 nm nano-object. As a result, these hybrid nanogels can simultaneously act as high-resolution biosensors for temperature sensing, fluorescent agents for tumor-cell imaging, and smart drug carriers for synergistic chemo-photothermal treatment. These multifunctional hybrid nanogels should promise a new efficient modality for broad applications in high-resolution temperature sensing-related techniques, as well as for in vivo animal models and future clinical trials in cancer diagnosis, therapy, and monitoring. We envision that the approach presented here may open new possibilities to bridge the unique properties of different materials to leverage research both fundamentally and practically, using a variety of interdisciplinary combinations.

4. Experimental Section

Materials: All chemicals were purchased from Aldrich. MEO_2MA, MEO_5MA (M_n = 300 g mol^{-1}) and PEGDMA ($M_n \approx$ 550 g mol^{-1}) were purified with neutral Al_2O_3. 2,2′-Azobisisobutyronitrile (AIBN) was purified by recrystallization from anhydrous ethanol. TMZ, $Zn(MAA)_2$, $HAuCl_4 \cdot 3H_2O$, NaCl, and trisodium citrate were used as received without further purification. The water used in all experiments was of Millipore Milli-Q grade.

Synthesis of ZnO@PEG Hybrid Nanogels: $Zn(MAA)_2$ (1.28 mmol), MEO_2MA (12.00 mmol), MEO_5MA, and PEGDMA (0.18 mmol) were dissolved in anhydrous ethanol (25 mL) in a 100 mL round-bottom flask equipped with a stirrer and a condenser. The solution was stirred and heated to 80 °C, and then AIBN (0.41 mmol) was added. After refluxing for 2 min, the solution turned milky white. NaOH (0.25 mL, 10 M)

© 2011 WILEY-VCH Verlag GmbH & Co. KGaA, Weinheim

aqueous solution was added into the reaction system and continuously refluxed for another 1 h. After cooling to room temperature, the product was purified by centrifugation (20 000 rpm, 30 min, 35 °C, Thermo Electron Co. Sorvall RC-6 PLUS superspeed centrifuge), redispersion in water, and 3 d dialysis (Spectra/Por molecularporous membrane tubing, cutoff 12 000–14 000) against water. Four ZnO@PEG hybrid nanogels were prepared by changing the feeding amount of MEO_5MA to 5.42, 9.16, 13.55, and 18.34 mmol, respectively.

Synthesis of ZnO-Au@PEG Hybrid Nanogels: The purified ZnO@PEG hybrid nanogels (50 mL) in a 150 mL glass vial were stirred in an ice water bath for 30 min, trisodium citrate (2.5 mL, 30 mmol L^{-1}) was then added dropwisely to the vial. $HAuCl_4$ solution (1 mL, 25 mmol L^{-1}) was slowly dropped into the above solution while vigorously stirring for 24 h at room temperature until the color was stable. During this period, the solution changed from light white to wine red and became transparent, which indicated that Au particles have been formed. The resulted ZnO-Au@PEG hybrid nanogels were purified with centrifugation/redispersion in water for three cycles, followed by 3 d of dialysis against very frequently changed water. Four samples were prepared with the variable feeding of MEO_5MA at 5.42 mmol (ZAG-1), 9.16 mmol (ZAG-2), 13.55 mmol (ZAG-3), and 18.34 mmol (ZAG-4).

Drug Loading and Release: TMZ was loaded into ZnO-Au@PEG hybrid nanogels by complexation. The pH value of hybrid nanogel (5 mL) was adjusted to 4.0 by using HCl solution (0.1 N). This dispersion was stirred in an ice water bath for 30 min. TMZ solution (500 μL, 1 mg mL^{-1}, pH = 2.0) was then added dropwisely to the vial. The hydrogen bonding complexation of TMZ molecules with PEG chains caused an immediate slightly cloudy solution. After stirring overnight, the suspension was centrifuged at 20 000 rpm for 30 min at 22 °C. To remove free TMZ, the precipitate was redispersed in HCl solution (5 mL, pH = 4.0), and further purified by repeated centrifugation and washing. All the upper clear solutions were collected, and the concentration of free TMZ was determined by UV–vis spectrometry at 328 and 260 nm, based on the linear calibration curve with $R^2 > 0.99$ measured using the TMZ solutions with known concentrations under the same condition. The amount of TMZ loaded into hybrid nanogels was calculated from the decrease in TMZ concentration. The loading content is expressed as the mass of loaded drug per unit weight of dried hybrid nanogels.

The in vitro release test of TMZ from ZnO-Au@PEG hybrid nanogels was evaluated by the dialysis method. A dialysis bag filled with purified TMZ-loaded hybrid nanogel dispersion (5 mL, pH = 4.0) was immersed in buffer solutions (50 mL, 0.005 M, pH = 7.4) at different temperatures. To examine the photothermal effects on the releasing rate, 5 min NIR (1.5 W cm^{-2}) irradiation at certain time intervals was applied to the releasing samples. The released TMZ outside of the dialysis bag was sampled at defined time period and assayed by UV–vis absorption at both 328 and 260 nm. Cumulative release is expressed as the total percentage of drug released through the dialysis membrane over time.

Incorporation of the Hybrid Nanogels into B16F10 Cells: Round glass coverslips were placed in wells of a 24-well plates and treated with 0.1% poly-L-lysine in phosphate buffered saline (0.100 M) for 40 min. Following the treatment, the solution was aspirated and the wells were washed with PBS three times each. Next, B16F10 cells (2×10^5 cell $well^{-1}$) were plated on the glass coverslips at 80% confluence in DMEM containing 10% FBS and 1% penicillin-streptomycin. After 24 h, different ZnO-Au@PEG hybrid nanogels (500 μL, 3.0 μg mL^{-1}) in serum-free DMEM were added to the marked wells. In a control well, serum-free DMEM (500 μL) was added. The plate was incubated at 37°C for 24 h. The medium was then aspirated and fresh serum-free DMEM was added to each well. Finally, the coverslips with cells were removed from the wells and mounted onto slides.

Cell Viability Evaluation: B16F10 cells (6×10^4 cell $well^{-1}$) were cultured in DMEM containing 10% FBS and 1% penicillin-streptomycin in a 96-well plate, and exposed to free TMZ, empty hybrid nanogels, and TMZ-loaded hybrid nanogels. To cover the high concentrations, the nanogels were concentrated and adjusted to an appropriate concentration in DMEM right before feeding into the well. Then, the cells were irradiated with 1.5 W cm^{-2} NIR light for 5 min for photothermal and chemo-photothermal treatments, while maintaining an average solution temperature of approximately 37 °C. For chemotherapy alone, the cells were not exposed to NIR light. The plate was incubated at 37 °C for 24 h. The medium was then aspirated, and these wells were washed three times using fresh serum-free DMEM. After that, 3-(4,5-dimethyl-2-thiazolyl)-2,5-diphenyltetrazolium bromide (MTT) solution (25 μL, 5 mg mL^{-1} in PBS) were added to the wells. After incubation for 2 h, the solution was aspirated and DMSO (100 μL) was added to each well to dissolve the formazan crystal, and the plate was sealed and incubated overnight at 37 °C with gentle mixing. Three portions of the solution obtained from each well were transferred to three respective wells of a 96-well plate. Cell viability was measured using a microplate reader at 570 nm. Positive controls contained no drug or nanogels, and negative controls contained MTT. Parallel wells (in triplicate) also contained only medium (no cells) and the same concentrations of hybrid nanogels.

Characterization: UV–vis–NIR absorption spectra were obtained on a Thermo Electron Co. Helios β UV–vis spectrometer. PL spectra of the hybrid nanogel dispersions at different temperatures were respectively obtained on a Jobin Yvon Co. FluoroMax-3 Spectrofluorometer equipped with a Hamamatsu R928P photomultiplier tube, calibrated photodiode for excitation reference correction from 200 to 980 nm, and an integration time of 1 s. To confirm all emissions, PL spectra were also recorded on a Varian Cary Eclipse Fluorescence spectrophotometer equipped with R928 photomultiplier tubes and self-optimized light filters. The pH values were measured on a Mettler Toledo SevenEasy pH meter. TEM images were taken on a FEI Tecnai transmission electron microscope at an accelerating voltage of 120 kV. Cell imaging were conducted on a confocal laser scanning microscopy (Leica TCS SP2 AOBS) equipped with a HC PL APO CS 20 × 0.7 DRY len, and a UV (405 nm) light as the light source. Dynamic light scattering (DLS) was performed on a 90Plus multi-angle particle sizing analyzer equipped with a BI-9000AT digital autocorrelator (Brookhaven Instruments, Inc.) to measure the R_h distributions. A He–Ne laser (35 mW, 659 nm) was used as the light source. All dispersions were passed through Millipore Millex-HV filters with a pore size of 0.80 μm to remove dust before the DLS measurements.

Supporting Information

Supporting Information is available from the Wiley Online Library or from the author.

Acknowledgements

We gratefully acknowledge financial support from the US Agency for International Development under the US–Pakistan Science and Technology Cooperative Program (PGA-P280422). We also thank Phyllis Langone at the CSI/IBR Center for Developmental Neuroscience for her help with cell culture.

Received: January 25, 2011
Published online: May 31, 2011

[1] a) D. Bardelang, M. B. Zaman, I. L. Moudrakovski, S. Pawsey, J. C. Margeson, D. Wang, X. Wu, J. A. Ripmeester, C. I. Ratcliffe, K. Yu, *Adv. Mater.* **2008**, *20*, 4517; b) S. Lim, C. Zhong, *Acc. Chem. Res.* **2009**, *42*, 798; c) A. M. Smith, S. M. Nie, *Nat. Biotechnol.* **2009**, *27*, 732; d) I. Tokarev, I. Tokarva, V. Gopishetty, E. Katz, S. Minko, *Adv. Mater.* **2010**, *22*, 1412.

[2] a) Y. D. Jin, X. H. Gao, *Nat. Nanotechnol.* **2009**, *4*, 571; b) M. Zacharria, B. Lamory, N. Chateau, *Nat. Photonics* **2011**, *5*, 24.

[3] a) K. Park, S. Lee, E. Kang, K. Kim, K. Choi, I. C. Kwon, *Adv. Funct. Mater.* **2009**, *19*, 1553; b) S. M. Lee, H. Park, K. H. Yoo, *Adv. Mater.* **2010**, *22*, 4049; c) J. Shi, A. R. Votruba, O. C. Farokhzad, R. Langer, *Nano Lett.* **2010**, *10*, 3223.

© 2011 WILEY-VCH Verlag GmbH & Co. KGaA, Weinheim

[4] a) X. Wang, X. Ren, K. Kahen, M. A. Hahn, M. Rajeswaran, S. Maccagnano-Zacher, J. Silcox, G. E. Cragg, A. L. Efros, T. D. Krauss, *Nature* **2009**, *459*, 686; b) H. Xiong, Y. Xu, Q. Ren, Y. Xia, *J. Am. Chem. Soc.* **2008**, *130*, 7522; c) P. Zhang, W. Liu, *Biomaterials* **2010**, *31*, 3087; d) J. P. Zimmer, S. Kim, S. Ohnishi, E. Tanaka, J. V. Frangioni, M. G. Bawendi, *J. Am. Chem. Soc.* **2006**, *128*, 2526; e) N. Pradhan, D. M. Battaglia, Y. Liu, X. G. Peng, *Nano Lett.* **2007**, *7*, 312.

[5] a) W. Wu, M. Aiello, T. Zhou, A. Berliner, P. Banerjee, S. Q. Zhou, *Biomaterials* **2010**, *31*, 3023; b) W. Wu, J. Shen, P. Banerjee, S. Q. Zhou, *Biomaterials* **2010**, *31*, 8371; c) W. Wu, T. Zhou, J. Shen, S. Q. Zhou, *Chem. Commun.* **2009**, 4390; d) W. Wu, T. Zhou, M. Aiello, S. Q. Zhou, *Biosens. Bioelectron.* **2009**, *25*, 2603.

[6] a) J. Zhang, S. Xu, E. Kumacheva, *J. Am. Chem. Soc.* **2004**, *126*, 7908; b) Y. Gong, M. Gao, D. Wang, H. Mhwald, *Chem. Mater.* **2005**, *17*, 2648; c) M. Agrawal, J. Rubio-Retama, N. E. Zafeiropoulos, N. Gaponik, S. Gupta, V. Cimrova, V. Lesnyak, E. Lopez-Cabarcos, S. Tzavalas, R. Rojas-Reyna, A. Eychmuller, M. Stamm, *Langmuir* **2008**, *24*, 9820.

[7] a) X. H. Huang, I. H. El-Sayed, W. Qian, M. A. El-Sayed, *J. Am. Chem. Soc.* **2006**, *128*, 2115; b) J. Nam, N. Won, H. Jin, H. Chung, S. Kim, *J. Am. Chem. Soc.* **2009**, *131*, 13639; c) N. J. Halas, *Nano Lett.* **2010**, *10*, 3816.

[8] a) Y. Cheng, A. C. Samia, J. D. Meyers, I. Panagopoulos, B. Fei, C. Burda, *J. Am. Chem. Soc.* **2008**, *130*, 10643; b) S. S. Agasti, A. Chompoosor, C. C. You, P. Ghosh, C. K. Kim, V. M. Rotello, *J. Am. Chem. Soc.* **2009**, *131*, 5728.

[9] a) M. S. Yavuz, Y. Cheng, J. Chen, C. M. Cobley, Q. Zhang, M. Rycenga, J. Xie, C. Kim, K. H. Song, A. G. Schwartz, L. V. Wang, Y. N. Xia, *Nat. Mater.* **2009**, *8*, 935; b) W. Wu, J. Shen, P. Banerjee, S. Q. Zhou, *Biomaterials* **2010**, *31*, 7555.

[10] a) C. Stefanadis, C. Chrysochoou, D. Markou, K. Petraki, D. B. Panagiotakos, C. Fasoulakis, A. Kyriakidis, C. Papadimitriou, P. K. Toutouzas, *J. Clin. Oncol.* **2001**, *19*, 676; b) V. P. Torchilin, *Pharm. Res.* **2006**, *24*, 1.

[11] C. Gota, K. Okabe, T. Funatsu, Y. Harada, S. Uchiyama, *J. Am. Chem. Soc.* **2009**, *131*, 2766.

[12] a) D. Peer, J. M. Karp, S. Hong, O. C. Farokhzad, R. Margalit, R. Langer, *Nat. Nanotechnol.* **2007**, *2*, 751; b) S. S. Agasti, S. Rana, M. Park, C. K. Kim, C. You, V. M. Rotello, *Adv. Drug Delivery Rev.* **2010**, *62*, 316.

[13] a) T. Mokari, E. Rothenberg, I. Popov, R. Costi, U. Banin, *Science* **2004**, *304*, 1787; b) T. Mokari, C. G. Sztrum, A. Salant, E. Rabani, U. Banin, *Nat. Mater.* **2005**, *4*, 855.

[14] a) B. Dubertret, M. Calame, A. J. Libchaber, *Nat. Biotechnol.* **2001**, *19*, 365; b) T. Pons, I. L. Medintz, K. E. Sapsford, S. Higashiya, A. F. Grimes, D. S. English, H. Mattoussi, *Nano Lett.* **2007**, *7*, 3157.

[15] O. Kulakovich, N. Strekal, A. Yaroshevich, S. Maskevich, S. Gaponenko, I. Nabiev, U. Woggon, M. Artemyev, *Nano Lett.* **2002**, *2*, 1449.

[16] a) X. Wang, C. J. Summers, Z. Wang, *Appl. Phys. Lett.* **2005**, *86*, 013111; b) X. Wang, X. Kong, Y. Yu, H. Zhang, *J. Phys. Chem. C* **2007**, *111*, 3836.

[17] F. Reith, S. L. Rogers, D.C. McPhail, D. Webb, *Science* **2006**, *313*, 233.

[18] H. Xiong, X. Zhao, J. Chen, *J. Phys. Chem. B* **2001**, *105*, 10169.

[19] a) L. Zhang, F. X. Gu, J. M. Chan, A. Z. Wang, R. S. Langer, O. C. Farokhzad, *Clin. Pharmacol. Ther.* **2008**, *83*, 761; b) V. Weissig, K. R. Whiteman, V. P. Torchilin, *Pharm. Res.* **1998**, *15*, 1552.

[20] a) A. Lukyanov, Z. Gao, L. Mazzola, V. P. Torchilin, *Pharm. Res.* **2002**, *19*, 1424; b) F. Alexis, E. Pridgen, L. K. Molnar, O. C. Farokhzad, *Mol. Pharm.* **2008**, *5*, 505.

[21] E. A. Meulenkamp, *J. Phys. Chem. B* **1998**, *102*, 5566.

[22] a) J. Lutz, K. Weichenhan, Ö. Akdemir, A. Hoth, *Macromolecules* **2007**, *40*, 2503; b) C. Chi, T. Cai, Z. B. Hu, *Langmuir* **2009**, *25*, 3814.

[23] a) L. M. Liz-Marzán, M. Giersig, P. Mulvaney, *Langmuir* **1996**, *12*, 4329; b) R. Contreras-Cáceres, A. Sánchez-Iglesias, M. Karg, I. Pastoriza-Santos, J. Pérez-Juste, J. Pacifico, T. Hellweg, A. Fernández-Barbero, L. M. Liz-Marzán, *Adv. Mater.* **2008**, *20*, 1666.

[24] a) S. R. Wuister, C. M. Doneg, A. Meijerink, *J. Am. Chem. Soc.* **2004**, *126*, 10397; b) A. M. Smith, A. M. Mohs, S. M. Nie, *Nat. Nanotechnol.* **2009**, *4*, 56.

[25] Y. Li, T. Tanaka, *J. Chem. Phys.* **1990**, *92*, 1365.

[26] C. E. Reese, A. V. Mikhonin, M. Kamenjicki, A. Tikhonov, S. A. Asher, *J. Am. Chem. Soc.* **2004**, *126*, 1493.

[27] a) C. Wu, S. Q. Zhou, *Phys. Rev. Lett.* **1996**, *77*, 3053; b) C. Wu, S. Q. Zhou, *Macromolecules* **1997**, *30*, 574; c) J. Lutz, Ö. Akdemir, A. Hoth, *J. Am. Chem. Soc.* **2006**, *128*, 13046.

[28] A. V. Bader, J. P. bader, *J. Cell Physiol.* **1976**, *87*, 33.

[29] a) F. Shen, L. A. Decosterd, M. Gander, S. Leyvraz, J. Biollaz, F. Lejeune, *J. Chromatogr. B* **1995**, *667*, 291; b) S. Baruchel, M. Diezi, D. Hargrave, D. Stempak, J. Gammon, A. Moghrabi, M. J. Coppes, C. V. Fernandez, E. Bouffet, *Eur. J. Cancer* **2006**, *42*, 2335.

[30] J. Siepmann, N. A. Peppas, *Adv. Drug Delivery Rev.* **2001**, *48*, 139.

[31] W. Jiang, B. Y. S. Kim, J. T. Rutka, W. C. W. Chan, *Nat. Nanotechnol.* **2008**, *3*, 145.

[32] G. S. Kwon, *Crit. Rev. Ther. Drug Carrier Syst.* **1998**, *15*, 481.

[33] G. M. Hahn, J. Braun, I. Har-kedar, *Proc. Natl. Acad. Sci. USA* **1975**, *72*, 937.

© 2011 WILEY-VCH Verlag GmbH & Co. KGaA, Weinheim